CHAPTER IV

SYNTHESIS AND CHARACTERIZATION OF M-MCM-48 (M = Cr, Ce) FROM SILATRANE VIA SOL-GEL PROCESS

4.1 Abstract

Metal (Chromium and Cerium) incorporated into MCM-48 framework is hydrothermally synthesized via sol-gel process without any additives and characterized by X-ray diffraction (XRD), N_2 adsorption/desorption, Scanning electron microscopy (SEM), Transmission electron microscopy (TEM), Diffuse reflectance UV-vis spectroscopy (DR-UV), and Thermogravimetric analysis (TGA). Results indicate that the materials possess a long-range ordered structure, high surface area, and narrow pore size distribution. SEM images illustrate the edge-truncated octahedron morphology of Cr-MCM-48 while Ce-MCM-48 preserves the truncated octahedron of the MCM-48 parent material. TEM images show the *Ia3d* pore structure after loading metals. Spectroscopic data confirm the existence of metals in the framework and extra-framework. At low Cr content, Cr-MCM-48 contains only Cr(VI) species while rich Cr content loading results in both the Cr(VI) and Cr(III) species. The hydrothermal stability of MCM-48 is enhanced by carefully incorporating metals into the parent material.

(**Keywords**: Sol-gel process; Cr-MCM-48; Ce-MCM-48; Hydrothermal stability)

4.2 Introduction

Since the 1992 discovery of mesoporous molecular sieves in the M41S family by Mobil's group [1, 2], these materials have attracted remarkable attention due to their high surface area, ordered pore structure array, and narrow pore size distribution [3]. Among them, MCM-48 is a more attractive candidate as a catalyst, catalyst support, adsorbent, or template for synthesis of advanced nanostructures, probably owing to its unique three-dimensional pore structure. However, these materials possess weak acidity and are deficient in necessary redox ability, thus exhibiting low activity when directly used as catalyst [4]. To obtain materials with high catalytic performance, many attempts have been made to incorporate a hetero-element, such as Cr, Ti, Ce, or V, to the silicate framework so as to enhance the acid and/or redox properties of the materials [5]. Among those hetero-atoms, Cr is attractive as a redox-active site for many chemical reactions. Consequently, in recent years many researchers have focused on the synthesis of Cr-containing mesoporous materials, including Cr-MCM-41 [6, 7], Cr-MCM-48 [8, 3, 9], Cr-MSU-1 [10, 11], and tested for selective oxidation reaction. Cerium (Ce) is also interesting in terms of catalytic applications since incorporation of Ce in the silica framework provides the Lewis and Bronsted acid sites which affect to the catalytic properties [12]. Hence, many researches focused on the incorporation of Ce in mesoporous materials, such as Ce-KIT-6 [12], Ce-MCM-48 [13, 14, 15], Ce-SBA-15 [16], and Ce-MCM-41 [17]. Besides the catalytic properties, the incorporation of hetero-atoms can also enhance hydrothermal stability, as compared to the pure siliceous mesoporous materials found in many reports [3, 15]. However, the synthesis of chromium or cerium-containing MCM-48 with highly ordered pore structure, high surface area as well as the truncated octahedron morphology using silatrane as silica source has not been reported.

In this study, we have expanded our previous work [18] by incorporating Cr and Ce into the MCM-48 framework. The synthesis of M-MCM-48 (where M = Cr and Ce) with various amounts of metals were investigated and characterized using powder XRD, N_2 adsorption/desorption, SEM, TEM, DR-UV, and TGA. In addition,

the influence of metal-incorporated MCM-48 on a hydrothermal stability was studied.

4.3 Experimental

4.3.1 Materials

Cr-MCM-48 and Ce-MCM-48 mesoporous materials were synthesized hydrothermally, using fumed silica (SiO_2, 99.8%, Sigma-Aldrich, USA), triethanolamine (TEA, Carlo Erba, Italy), triethylenetetramine (TETA) (Facai, Thailand), ethylene glycol (EG, J.T. Baker, USA), acetronitrile (Labscan, Thailand), sodium hydroxide (NaOH, Labscan, Asia), cetyltrimethylammonium bromide (CTAB, Sigma-Aldish, Denmark), chromium(III)nitrate nonahydrate (Himedia, India), and cerium(IV) hydroxide (Sigma-Aldish, U.S.A.)

4.3.2 Synthesis of M-MCM-48 (M = Cr,Ce)

The Cr-containing MCM-48 materials were synthesized using our previously published method [18]. CTAB, used as a structure-directing agent, was dissolved in a solution containing water and 2M NaOH. The mixture was stirred continuously with slight heating to dissolve CTAB. Our homemade silatrane, used as a silica source and prepared according to Wongkasemjit's synthetic method [19], was added into the CTAB mixture, followed by adding a required amount of 0.3M chromium nitrate solution under continuous stirring for 1 h. The molar composition of the gel was 1.0 SiO_2:0.3CTAB:0.50NaOH:62.0H_2O:xCr, where $0.005 \leq x \leq 0.1$. The process of synthesizing Ce-MCM-48 was similar to that of Cr-MCM-48, except the metal precursor. In this case, we used homemade cerium glycolate synthesized according to a procedure described elsewhere [20]. After the silatrane was added to the solution, a required amount of cerium glycolate was added into the solution under continuous stirring for 1 h. The molar composition of the gel was 1.0 SiO_2:0.3CTAB:0.50NaOH:62.0H_2O:yCe, where $0.01 \leq y \leq 0.09$. The resulting mixture was transferred to a Teflon-lined stainless steel autoclave and treated at 140 °C for 16 h. The resulting solid product was collected by filtration and dried overnight at ambient conditions. The removal of all organics was performed by

calcination at 550 °C for 6 h (Carbolite, CFS 1200, Hope Valley, U.K.) at a heating rate of 0.5 °C/min to obtain mesoporous M-MCM-48. All of the obtained Cr-MCM-48 samples varied in color from yellow to green, depending on the amount of Cr, while the color of the obtained Ce-MCM-48 was only yellow. The samples prepared were denoted as Cr-MCM-48-(x) and Ce-MCM-48-(y), where x and y were the ratios of Cr/Si and Ce/Si in the solution, respectively. The metal-free MCM-48 was synthesized with the same procedure to compare.

4.3.3 Characterization

The M-MCM-48 products were characterized using an XRD (Rigaku, Japan) and CuKα radiation in the range of $2\theta = 2°–60°$ at a scanning speed of 1 °C/min, 40 kV, and 30 mA. The morphology of products was carried out by a field emission scanning electron microscope (FE-SEM, Hitachi/S-4800). The order of mesopores was investigated using a TEM (JEOL 2010F). The specific surface area and average pore size were estimated by the Brunauer-Emmett-Teller (BET) method on a Quantasorb JR instrument (Mount Holly, NJ). DRUV spectra of samples were recorded from 200 to 800 nm on a Shimadzu UV-2550 spectrophotometer using $BaSO_4$ as a reference. Thermogravimetric analysis of materials was carried out on Perkin-Elmer instruments using a heating rate of 10 °C/min from room temperature to 650 °C in a nitrogen atmosphere.

4.3.4 Hydrothermal Stability Test

Following the method of Jun *et al.* [21], 0.1g of a calcined sample in 100 mL of distilled water was boiled in a round-bottom flask connected with a reflux condenser for 12 h. The sample was recovered by filtration and drying in air overnight for further characterization. Then, the XRD pattern was obtained and compared with the same sample before the heat treatment to determine the hydrothermal stability.

4.4 Results and Discussion

4.4.1 XRD

According to Table 1, unit cell parameter and d-spacing of the as-synthesized samples slightly increased with an increase in Cr/Si ratio, indicating that Cr had slightly or no influence on the silica framework [6]. This can be explained in terms of the incorporation of a larger cation, such as Cr(III) (0.76 Å) in the tetrahedral geometry of Si (0.40 Å), as a consequence of the expansion of the unit cell. However, the small expansion in a_0 and higher d values were noticed, which could imply that the chromium species was filled in the pores, in agreement with those described by Sakthivel and Selvam [6]. Nevertheless, the structure of MCM-48 was preserved after loading of Cr, as can be noticed in the XRD patterns in Fig. 4.1(a). Furthermore, the as-synthesized samples were pale green in color and changed to yellow after calcination. This could suggest that the trivalent chromium ions in octahedral geometry were changed to the higher valent chromium ions, viz., chromate and/or polychromate ions, in the tetrahedral environment [6]. These results were consistent with the decrease in a_0 values of calcined samples in Table 4.2, which may be attributed to the short double bond Cr=O in Cr_2O_3 or Cr_2O_5. As mentioned earlier, it is also indicated that the calcined samples were composed mostly of Cr(VI) or Cr(V) species, as compared to a lower valent [22]. However, the structural alteration was obtained in increasing the Cr/Si ratio higher than 0.01 (not shown). This might be a result of the high Cr content affecting the surfactant-silicate interaction which was involved in the assembly of the surfactant and silicate species [23]. Similar to the work of Shao *et al.*, the less-ordered structure at high Cr content was obtained due to the lower peak intensity and unresolved patterns, probably due to the partially collapsed structure [3]. Interestingly, for the first time, we found in our case that the structure was changed from MCM-48 to MCM-41 as Cr content increased.

Fig. 4.1(b) exhibited the XRD patterns of calcined Cr-MCM-48 samples over the range of 10°–60°. The addition of small diffraction peaks at 2θ = 24.5°, 33.6°, 36.2°, and 54.8° belonging to the hexagonal phase of Cr_2O_3 was detected at a Cr/Si ratio above 0.05 [11]. It is indicated that all Cr/Si ratios below

0.05 resulted in Cr incorporated into MCM-48 framework. Additionally, there was no Cr_2O_3 metal oxide diffraction peaks at high-angle XRD patterns of the samples having the Cr/Si ratio in the range of 0.005–0.03, implying that the Cr atoms were indeed in the framework of MCM-48 structure [24].

Considering the XRD patterns of calcined Ce-MCM-48, all samples provided a well-resolved XRD pattern of MCM-48 even at high Ce loadings. It could be inferred that the incorporation of cerium in the silica framework did not change the cubic *Ia3d* pore structure. Moreover, the secondary peaks (2θ = 3°–6°) were obviously seen in all samples, as shown in Fig. 4.2(a). It could be pointed out that the long-range order of the MCM-48 structure was obtained [25]. As compared to the study of Shao *et al.* [15], who synthesized the long-range ordered Ce-MCM-48 by the aid of fluoride ions with 0.1 molar ratio, our results were obtained with no addition of any ions. The unit cell parameters and the d-spacing of both as-synthesized and calcined Ce-MCM-48 were shown in Tables 4.1 and 4.2, respectively.

The XRD patterns of the calcined Ce-MCM-48 materials, over the range of 10°–60°, are demonstrated in Fig. 4.2(b). The MCM-48 provided the pattern corresponding to the amorphous-like nature of silica [26]. No additional peaks appeared for all the materials prepared with the Ce/Si ratios in the range of 0.01–0.03. Even over the Ce/Si range of 0.05–0.09, only a few weak broad peaks could barely be noticed around the 2 theta of 28.55°, 47.47° and 56.33°, corresponding to the (111), (220) and (311) planes, respectively, for the main characteristic lines of ceria (CeO_2) structure. These results indicate that the fine, small particles of ceria might be formed within MCM-48, as described by Khalil [27]. He synthesized Ce-containing MCM-41 prepared via a direct and non-hydrothermal method with 5% and 10% (w/w) of CeO_2/silica and found that the cerium inserted into the framework of MCM-41 and/or the formation of finely divided ceria nanoparticles on the wall of MCM-41 was obtained. The intensity of ceria-characteristic peaks gradually increased with an increase in the Ce content, meaning that the amount of CeO_2 in the channel or in the extra-framework increased, as also reported by Wangcheng *et al.* [13]. Additionally, they obtained low intense diffractions of the secondary peaks even at low Ce content (Ce/Si = 0.02), implying that there was no long-range ordered

structure. In contrast to our work, the highly ordered structure was sustained even at high Ce loadings. This might be a result from the presence of the by-products, EG and TEA, generated from the hydrolysis of cerium glycolate and silatrane precursors, respectively. Both EG and TEA were able to enhance the ordering of MCM-48 structure, as discussed elsewhere [18].

4.4.2 Hydrothermal Stability Test

The XRD patterns (not shown) of the calcined MCM-48 after refluxing in boiling water for 12 h indeed lost its mesoporous-ordered structure, as described by Shao *et al.* [15]. Generally, the hydrolysis rate of Si-O-Si bonds is quite fast, resulting in the collapsed structure, if the pore walls of the materials are thin or have less polymerization [3]. However, the XRD pattern of calcined Cr-MCM-48 samples (not shown) exhibited a partly maintained mesoporous structure when compared to the complete loss of peaks in the MCM-48. This could imply that the incorporation of Cr to the structure was able to enhance the hydrothermal stability of MCM-48, as explained in terms of the higher resistance to water attack of the Si-O-Cr bonds compared to the Si-O-Si bonds [15]. A similar effect was found by Xia *et al.* [28, 29] who incorporated Al into mesoporous materials.

In contrast to the calcined Ce-MCM-48 materials with all Ce/Si ratios, after refluxing the samples in boiling water for 12 h, the results showed that most of the samples could not preserve the structure of MCM-48 (XRD patterns not shown), excluding 0.01 Ce/Si ratio. A structure of Ce-MCM-48-(0.01) was not completely lost, as compared to others. A similar observation was found in the work of Shao *et al.* [15], who explained in terms of the formation of Si-O-Ce bonds, which possessed more resistance to water attack than the Si-O-Si bonds, and high Ce contents could not efficiently enhance this property. They, thus, suggested that the structure ordering was considerably destroyed at the high Ce contents, leading to the decrease of hydrothermal stability.

4.4.3 N_2 Adsorption and Desorption Isotherms

The N_2 adsorption and desorption isotherms in Fig. 4.3 were typical type IV isotherms in the IUPAC classification. The isotherms exhibited a sharp curve

in the region of P/P_0 = 0.3–0.4, indicating a uniform pore size and highly ordered pore structure. These results were in harmony with the XRD patterns (Fig. 4.1a), showing a well-resolved secondary diffraction above 3.5 degrees of 2-theta, corresponding to a highly long-range order of these materials. Furthermore, according to Figs. 4.3 and 4.4, there is no hysteresis loop in the isotherms due to the absent of the capillary condensation in the materials with the pore diameter in the range of 2.27-2.47 nm. In addition, the inflection became less sharp with an increase in the amount of Cr in the materials, meaning that the well-ordered mesoporous structure could be destroyed by increasing the Cr content. Similar results were obtained by incorporation of Cr into MCM-41 [24]. Table 4.2 presents the characteristics of materials, viz., surface area, pore volume, and pore diameter. Interestingly, Cr-MCM-48-(0.005) and Cr-MCM-48-(0.01) have extremely high surface areas of 1,511 and 1,477 m^2/g, respectively, and a very narrow pore size distribution with a pore size of 2.27 and 2.30 nm, respectively. A decrease in the surface area with an increase in the Cr content was similar to the Cr-MCM-48 synthesized by Shao *et al.* [3], using a molar composition of the final gel mixture of $1.0TEOS:0.65CTAB:0.5NaOH:62H_2O:xCr(NO_3)_3.9H_2O$ where x = 0.005–0.04; or similar to Ga- or Al-containing MCM-41 [30, 31].

In the case of the calcined Ce-MCM-48 materials, the results revealed a decrease in surface area from 1,571 and 1,062 m^2/g as the Si/Ce ratio was increased from 0.01 to 0.09 (see Table 4.2), similar to the incorporation of Cr. Generally, an increase of the pore wall thickness is known to increase hydrothermal stability [21]. In our case, both Cr- and Ce- incorporated MCM-48, providing a thicker wall thickness, should give a positive effect to the hydrothermal stability. The materials also possessed the long plateau at higher relative pressure (see Figs. 4.3 and 4.4), implying that there was no pore filling after P/P_0 = 0.3, relating to wider mesopores [27]. Furthermore, the pore volume also decreased with an increase in the metal content, resulting in irregularity of mesopores, as described by Prabhu *et al.* [12]. Due to the steep of the capillary step in all samples, a narrow pore size distribution with diameters of 2.41–2.47 nm was thus achieved.

In general, the unit cell parameter (a_0) and the d-spacing should increase with an increase in the amount of heteroatoms into the silicate framework

[13, 24]. Many authors suggested that the M-O bond distance was longer than the Si-O one, leading to an increase in those parameters, as a result, knowing the presence of metal atoms in the framework of porous materials. In our case, the a_0 and the d-spacing decreased as metals were introduced into the materials, meaning that our results were not in agreement with those suggested elsewhere, but they were consistent with the study of Liu *et al.* [10]. They synthesized Cr-MSU-1, and the results showed that the d-spacing of the Cr-MSU-1 was not always larger than that of MSU-1. According to the explanation of Liu *et al.* [10], the higher degree of freedom of the system and the larger Cr-O bond, compared to the Si-O bond, should both contribute to the slight difference in the repeat distance in pure MSU-1 and Cr-MSU-1. This explanation could be supported by Arnold *et al.* [32] who synthesized V-MCM-41 and postulated that the bond distance and bond angle in mesoporous metallosilicate materials had a higher degree of freedom, as compared to the crystalline materials. They also suggested that MCM-41 was not a crystalline material and an alteration of repeat distance could not be directly compared with those crystalline materials.

4.4.4 DR-UV -Vis Spectroscopy

Generally, this technique is a very sensitive tool for characterizing metal ion coordination of metal containing zeolites to provide valuable information about the presence of metal ions in the framework and/or extra-framework [27]. Fig. 4.5 depicts the DR-UV-Vis spectra of calcined Cr-MCM-48 and Ce-MCM-48 with different Cr and Ce contents, respectively. All the spectra of the calcined Cr-MCM-48 with different Cr/Si ratios showed two bands around 260 and 350 nm. These absorption bands are generally assigned to O $\rightarrow$ Cr (VI) charge transfers of the chromate species [3]. The Cr(VI) polychromates at around 440 nm also existed in the materials. Moreover, the two typical bands of octahedral Cr(III) at 445 and 595 nm were found in the spectra of the calcined Cr-MCM-48(x) where $0.05 \leq x \leq 0.1$, consistent with the wide angle XRD results shown in Fig. 4.1(a). Hence, only Cr (VI) chromate was found in Cr-MCM-48 samples with low Cr loading, but the samples synthesized at higher Cr loading contained both Cr (VI) chromate and Cr (III) species.

As for Ce-MCM-48 samples, in general, the position of ligand-to-metal charge-transfer ($O^{2-} \rightarrow Ce^{4+}$) spectra depends on the ligand field symmetry surrounding the Ce center, and the electronic transitions from oxygen to a tetracoordinated Ce^{4+} require higher energy than a hexacoordinated one [15]. According to the spectra in Fig. 4.5, there was a weak broad absorption band at 200–300 nm and an intense band at around 350 nm, appearing for all Ce/Si ratios, and the increasing band intensities were found with an increase in the Ce content. Therefore, the absorption bands at those positions related to the presence of Ce^{4+} species with tetracoordination in the samples. Additionally, there was no absorption band at a higher wavelength (405 nm) corresponding to the hexacoordinated Ce^{4+} of CeO_2, as described in Wangcheng's work [13]. It could be concluded that much a higher amount of the tetracoordinated Ce in Ce-MCM-48 was present in the MCM-48 framework than those reported elsewhere [13, 15].

4.4.5 TGA

Weight losses for all synthesized samples were observed in the TGA plots (Fig. 4.6a). All Cr-MCM-48 samples revealed typical weight loss patterns, as reported elsewhere [33, 34]. It could be divided into three stages: the first stage attributed to the loss of physisorbed water below 100°C, the second one belonged to the removal of organic components at a temperature below 350°C and the last one at 350–600°C corresponded to the removal of carbon residues. Furthermore, the different features on the TGA curves of the Cr-MCM-48 and the pure MCM-48, might indicate the interaction between the incorporated Cr component and the surfactant molecules [34]. Similar observation was also reported by Kawi *et al.*, who synthesized MCM-48 supported Cr by introduction of chromium chloride during gel preparation of hydrothermal synthesis of MCM-48.

TGA curves of the synthesized Ce-MCM-48 in all Ce/Si ratios provided weight loss patterns similar to the pure MCM-48 as illustrated in Fig. 4.6b. The weight loss steps occurred through the temperature range, as described above.

4.4.6 FE-SEM

When more chromium was loaded in the MCM-48 supported with a Cr content of 0.005 and 0.01 mol, it was the first time we were able to observe the morphology change of calcined samples from the truncated octahedron of MCM-48 (see Fig. 4.7a) to the edge-truncated octahedron [35], implying that the chromium incorporated in MCM-48 affected the morphology of material, as shown in Fig. 4.7b, c. Our results were consistent with the study of Jha *et al.* [23], who obtained differences in the morphology of samples after incorporating various metals into MCM-41. The M-MCM-41 (M = Ti, V, Cr) showed spongy, flower-like, and agglomerated structures, respectively. These might be attributed to the presence of foreign ions in the synthesis gel, changing the surfactant-silicate interactions affected by the nature of metal source used [23]. These results are also in good agreement with those obtained by Parvulescu *et al.* [36]. They noticed that the morphological structure of MCM-41 surface could be modified by various metal ions. Furthermore, the enlargement of our samples (see Fig. 4.7d) revealed the primary particles of around 20 nm agglomerating to bigger edge-truncated octahedral particles in Fig. 4.7a and b. Similar observation was found in the calcined Ce-MCM-48 samples with all Ce/Si ratios, but the parent truncated octahedral MCM-48 still remained, as shown in Fig. 4.8.

4.4.7 TEM

TEM images of the calcined Cr-MCM-48-(0.005) with the incident direction along [100] and [432] (Fig. 4.9a, b) were similar to the study of Alfredsson and Anderson [37], demonstrating that the pore structure along this direction was a uniform channel system. From Fig. 4.9c, d, TEM images of the calcined Cr-MCM-48-(0.01) with the incident along [100] and [100] projection not only exhibited a uniform pore structure, but also reflected the structure of the pore channel. All TEM images agreed well with the XRD results given in Fig. 4.1a.

Fig. 4.10 illustrates the TEM images of Ce-MCM-48-(y), where y= 0.01, 0.05, 0.09 with the incident direction along [531], [100] and [111], respectively. They all indicated the *Ia3d* symmetry, as reported elsewhere [38, 18]. These results can confirm that the introduction of Ce does not damage the silica

framework, and the pore structure is still maintained the cubic Ia3d symmetry even at a high Ce content. Besides, the long-range ordered structures were obtained, confirming the XRD patterns in Fig. 4.2a.

4.5 Conclusions

In summary, the chromium- and cerium-incorporated MCM-48 were successfully synthesized by hydrothermal technique. They retained not only a long-range ordered structure of materials, but also their high surface area with a narrow pore size distribution after the incorporation of metal. The spectroscopic characterizations confirmed that Cr-MCM-48 contained Cr(VI) species at a low Cr content while both of the Cr(VI) and Cr(III) species existed in the rich Cr content. Ce-MCM-48 with all Ce contents showed the presence of Ce^{4+} tetracoordination in the framework in DRUV while the wide-angle XRD results indicated the existence of CeO_2 crystallites in the extra-framework at high Ce content. The morphology of metal-MCM-48 depended on the metal incorporated, in which the Cr-MCM-48 provided the edge-truncated octahedron morphology whereas the Ce-MCM-48 preserved the parent material shape. The hydrothermal stability for both metal-incorporated MCM-48 materials relied on the amount of metal loading.

4.6 Acknowledgements

This research is financially supported by the Thailand Research Fund and the Center for Petroleum, Petrochemicals, and Advanced Materials, Chulalongkorn University, Thailand. The authors would like to thank Mr. John M. Jackson for English proofreading.

4.7 References

[1] Kresge, C.T., Leonowicz, M.E., Roth, W.J., Vartuli, J.C., and Beck, J.S. (1992) Ordered mesoporous molecular sieves synthesized by a liquid-crystal template mechanism. Nature, 359, 710.

[2] Beck, J.S., Vartuli, J.C., Roth, W.J., Leonowicz, M.E., Kresge, C.T., Schmitt, K.D., Chu, C.T.W., Olson, D.H., Sheppard, E.W., McCullen, S.B., Higgins, J.B., and Schlenker, J.L. (1992) A new family of mesoporous molecular sieves prepared with liquid crystal templates. J. Am. Chem. Soc., 114, 10834.

[3] Shao, Y., Wang, L., Zhang, J., and Anpo, M. (2008) Synthesis and characterization of high hydrothermally stable Cr-MCM-48. Micropor. Mesopor. Mater., 109, 271–277.

[4] Vinu, A., Srinivasu, P., Miyahara, M., and Ariga, K. (2006) Preparation and Catalytic Performances of Ultralarge-Pore Ti-SBA-15 Mesoporous Molecular Sieves with Very High Ti Content. J. Phys. Chem. B, 110, 801-806.

[5] Corma, A. (1997) From Microporous to Mesoporous Molecular Sieve Materials and Their Use in Catalysis. Chem. Rev., 97, 2373-2420.

[6] Sakthivel, A. and Selvam, P. (2002) Mesoporous (Cr)MCM-41:A Mild and Efficient Heterogeneous Catalyst for Selective Oxidation of Cyclohexane. J. Catal., 211, 134–143.

[7] Samanta, S., Mal, N.K., and Bhaumik, A. (2005) Mesoporous Cr-MCM-41: An efficient catalyst for selective oxidation of cycloalkanes. J. Mol. Catal. A Chem., 236, 7–11.

[8] Laha, S.C. and Gläser, R. (2007) Characterization and catalytic performance of [Cr]MCM-41 and [Cr]MCM-48 prepared by either classical or microwave heating. Micropor. Mesopor. Mater., 99, 159–166.

[9] Sakthivel, A., Dapurkar, S.E., and Selvam, P. (2001) Mesoporous (Cr)MCM-41 and (Cr)MCM-48 Molecular Sieves: Promising Heterogeneous Catalysts for Liquid Phase Oxidation Reactions. Catal. Lett., 7, 155–158.

[10] Liu, L., Hi, L., and Zhang, Y. (2006) Effect of Synthesis Parameters on the Chromium Content and Catalytic Activities of Mesoporous Cr–MSU-x Prepared under Acidic Conditions. J. Phys. Chem. B, 110, 15478–15485.

[11] Liu, H., Wang, Z., Hu, H., Liang, Y., and Wang, M. (2009) Synthesis and characterization of Cr-MSU-1 and its catalytic application for oxidation of styrene. J. Solid. State. Chem., 182, 1726–1732.

[12] Prabhu, A., Kumaresan, L., Palanichamy, M., and Murugesan, V. (2010) Cerium-incorporated cage-type mesoporous KIT-6 materials: Synthesis, characterization and catalytic applications. Appl. Catal. A., 374, 11–17.

[13] Wangcheng, Z., Guanxhong, L., Yanglong, F., Yun, G., Yanqin, W., Yunsong, W., Zhigang, Z., and Xiaohui, L. (2008) Synthesis of cerium-doped MCM-48 molecular sieves and its catalytic performance for selective oxidation of cyclohexane. J. Rare Earths, 26, 515–522.

[14] Wang, L., Shao, Y., Zhang, J., and Anpo, M. (2006) Fast Synthesis of Si- and Ce-MCM-48 Mesoporous Molecular Sieve with Hydrothermal Stability. Chem. Lett., 35, 70–71.

[15] Shao, Y., Wang, L., Zhang, J., and Anpo, M. (2005) Synthesis of Hydrothermally Stable and Long-Range Ordered Ce-MCM-48 and Fe-MCM-48 Materials. J. Phys. Chem. B, 109, 20835–20841.

[16] Dai, Q., Chen, G., Wang, X., and Lu, G. (2007) Direct synthesis of cerium-incorporated SBA-15 mesoporous molecular sieves. Stud. Surf. Sci. Catal., 165, 81–84.

[17] Kadgaonkar, M.D., Laha, S.C., Pandey, R.K., Kumar, P., Mirajkar, S.P., and Kumar, R. (2004) Cerium-containing MCM-41 materials as selective acylation and alkylation catalysts. Catal. Today, 97, 225–231.

[18] Longloilert, R., Chaisuwan, T., Luengnaruemitchai, A., and Wongkasemjit, S. (2011) Synthesis of MCM-48 from silatrane via sol–gel process. J. Sol. Gel. Sci. Technol., 58, 427–435.

[19] Phiriyawirut, P., Magaraphan, R., Jamieson, A.M., and Wongkasemjit, S. (2003) Morphology study of MFI zeolite synthesized directly from silatrane and alumatrane via the sol–gel process and microwave heating. Micropor. Mesopor. Mater., 64(1–3), 83–93.

[20] Ksapabutra, B., Gulari, E., and Wongkasemjit, S. (2004) One-pot synthesis and characterization of novel sodium tris(glycozirconate) and cerium glycolate precursors and their pyrolysis. Mater. Chem. Phys., 88, 34–42.

[21] Jun, S., Kim, J.M., Ryoo, R., Ahn, Y.S., and Han, M.H. (2000) Hydrothermal stability of MCM-48 improved by post-synthesis restructuring in salt solution. Micropor. Mesopor. Mater., 41, 119–127.

[22] Wang, L., Wang, L., and Zhang, J. (2009) Direct synthesis of Cr-MCM-48-like large pore mesoporous silica. J. Mater. Sci., 44, 6512–6518.

[23] Jha, R.K., Shylesh, S., Bhoware, S.S., and Singh, A.P. (2006) Oxidation of ethyl benzene and diphenyl methane over ordered mesoporous M-MCM-41 (M = Ti, V, Cr): Synthesis, characterization and structure–activity correlations, Micropor. Mesopor. Mater., 95, 154–163.

[24] Shen, S. and Guo, L. (2000) Hydrothermal synthesis, characterization, and photocatalytic performances of Cr incorporated, and Cr and Ti co-incorporated MCM-41 as visible light photocatalysts for water splitting. Cat. Today, 129, 414–420.

[25] Kim, W.J., Yoo, J.C., and Hayhurst, D.T. (2000) Synthesis of hydrothermally stable MCM-41 with initial adjustment of pH and direct addition of NaF. Micropor. Mesopor. Mater., 39, 177.

[26] Kaneda, M., Tsubakiyama, T., Carlsson, A., Sakamoto, Y., Ohsuna, T., and Terasaki, O. (2002) Structural Study of Mesoporous MCM-48 and Carbon Networks Synthesized in the Spaces of MCM-48 by Electron Crystallography. J. Phys. Chem. B, 106, 1256–1266.

[27] Khalil, K.M.S. (2007) Cerium modified MCM-41 nanocomposite materials via a nonhydrothermal direct method at room temperature. J. Colloid. Interface. Sci., 315, 562–568.

[28] Xia, Y. and Mokaya, R. (2003) On the Hydrothermal Stability of Mesoporous Aluminosilicate MCM-48 Materials. J. Phys. Chem. B, 107, 6954-6960.

[29] Xia, Y. and Mokaya, R. (2004) Aluminosilicate MCM-48 materials with enhanced stability via simple post-synthesis treatment in water. Micropor. Mesopor. Mater., 68, 1-10.

[30] Cheng, C., He, H., Zhou, W., Klinowski, J., Goncalves, J., and Gladden, L. (1996) Synthesis and Characterization of the Gallosilicate Mesoporous Molecular Sieve MCM-41. J. Phys. Chem., 100, 390-396.

[31] Luan, Z., He, H., Zhou, W., Cheng, C., and Klinowski, J. (1995) Effect of structural aluminium on the mesoporous structure of MCM-41. J. Chem. Soc. Faraday. Trans., 9, 2955-2959.

[32] Arnold, A.B.J., Niederer, J.P.M., Niessen, T.E.W., and Hölderich, W.F. (1999) The influence of synthesis parameters on the vanadium content and pore size of [V]-MCM-41 materials. Micropor. Mesopor. Mater., 28, 353-360.

[33] Subrahmanyam, C., Louis, B., Rainone, F., Viswanathan, B., Renken, A., and Varadarajan, T.K. (2003) Catalytic oxidation of toluene with molecular oxygen over Cr-substituted mesoporous materials. Appl. Catal. A., 241, 205–215.

[34] Kawi, S. and Te, M. (1998) MCM-48 supported chromium catalyst for trichloroethylene oxidation. Catal. Today, 44, 101–109.

[35] Breen, T.L., Tien, J., Oliver, S.R.J., Hadzic, T., and Whitesides, G.M. (1999) Design and Self-Assembly of Open, Regular, 3D Mesostructures. Science, 284, 950-951.

[36] Pârvulescu, V., Anastasescu, C., and Su, B. L. (2004) Bimetallic Ru-(Cr, Ni, or Cu) and La-(Co or Mn) incorporated MCM-41 molecular sieves as catalysts for oxidation of aromatic hydrocarbons. J. Mol. Catal. A Chem., 211(1–2), 143-148.

[37] Alfredsson, V. and Anderson, W.M. (1996) Structure of MCM-48 Revealed by Transmission Electron Microscopy. Chem. Mater., 8, 1141–1146.

[38] Ohsuna, T., Sakamoto, Y., Terasaki, O., and Kuroda, K. (2011) TEM image simulation of mesoporous crystals for structure type identification. Solid. State. Sci., 13, 736–744.

Table 4.1 The unit cell parameter (a_0, calculated by $a_0 = d_{211}(6)^{1/2}$) and the d spacing of all synthesized samples with different chromium and cerium contents

Sample	M/Si (M=Cr,Ce) (mol)	a_0 (nm)	d-spacing (nm)
MCM-48	∞	9.45	3.86
Cr-MCM-48	0.005	9.49	3.88
Cr-MCM-48	0.01	9.66	3.94
Ce-MCM-48-(0.01)	0.01	9.53	3.89
Ce-MCM-48-(0.03)	0.03	9.58	3.91
Ce-MCM-48-(0.05)	0.05	9.79	4.00
Ce-MCM-48-(0.07)	0.07	9.71	3.96
Ce-MCM-48-(0.09)	0.09	9.75	3.98

Table 4.2 The characteristics of the calcined samples with a molar gel composition of $1.0SiO_2$:0.3CTAB:0.50NaOH:$62.0H_2O$:xCr or yCe, where $0 \leq x \leq 0.01$ and $0 \leq y \leq 0.09$ (a_0 was calculated by $d_{211}(6)^{1/2}$ and wall thickness was calculated by $a_0/3.0919$ – pore diameter/2)

Sample	S_{BET} (m^2/g)	Pore volume (cm^3/g)	Pore diameter (nm)	a_0 (nm)	d-spacing (nm)	Wall thickness (nm)
MCM-48	1,711	1.14	2.67	8.66	3.53	1.47
Cr-MCM-48-(0.005)	1,511	0.86	2.27	8.42	3.44	1.60
Cr-MCM-48-(0.01)	1,477	0.85	2.30	8.45	3.45	1.59
Ce-MCM-48-(0.01)	1,581	0.95	2.41	8.39	3.42	1.51
Ce-MCM-48-(0.03)	1,286	0.78	2.42	8.49	3.46	1.54
Ce-MCM-48-(0.05)	1,183	0.72	2.44	8.45	3.45	1.51
Ce-MCM-48-(0.07)	1,028	0.62	2.41	8.59	3.51	1.58
Ce-MCM-48-(0.09)	1,062	0.66	2.47	8.52	3.48	1.52

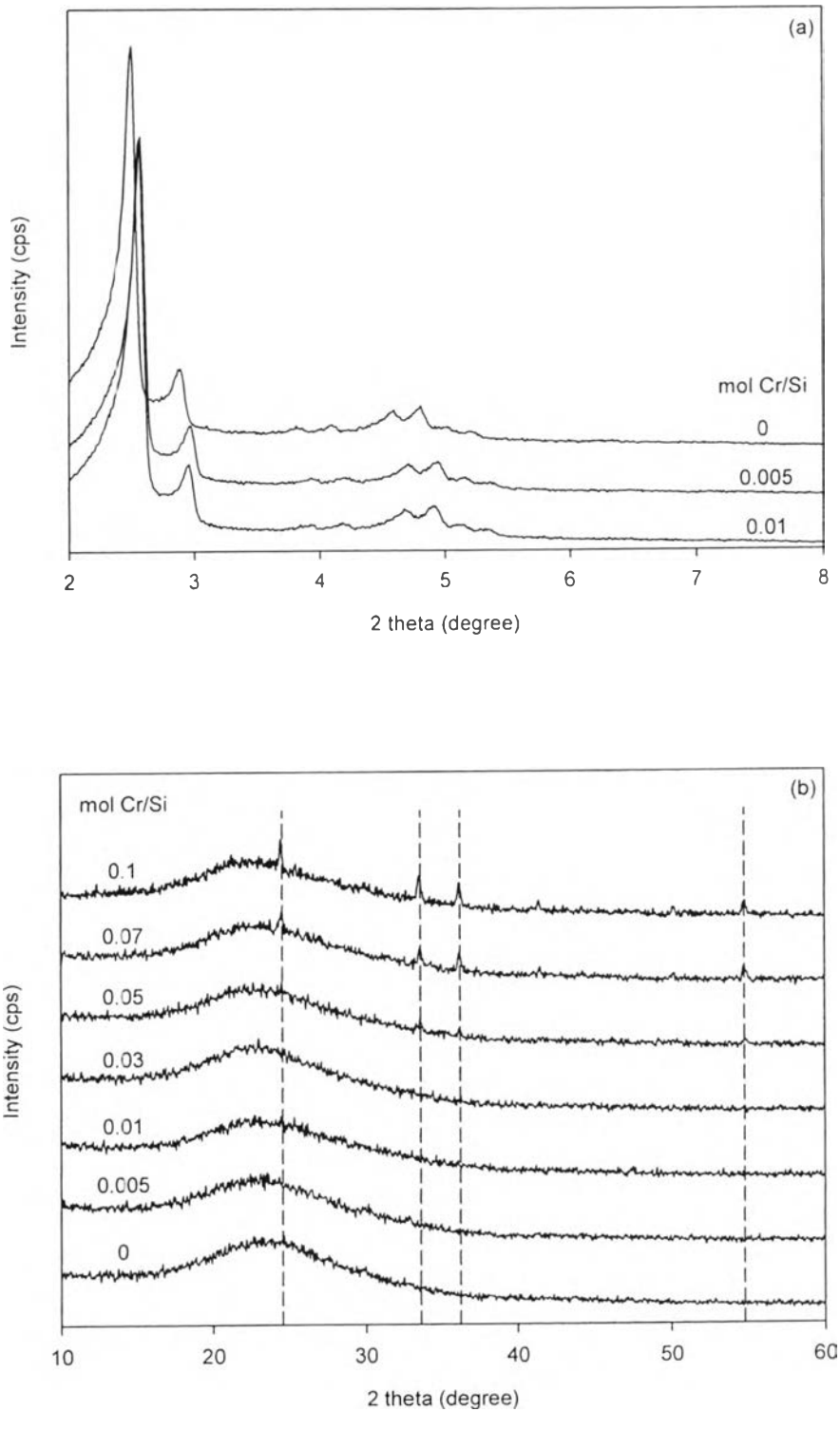

Figure 4.1 The XRD patterns of the calcined Cr-MCM-48 samples with different Cr contents over the range of (a) 2 theta = 2°–8° and (b) 2 theta = 10°–60°.

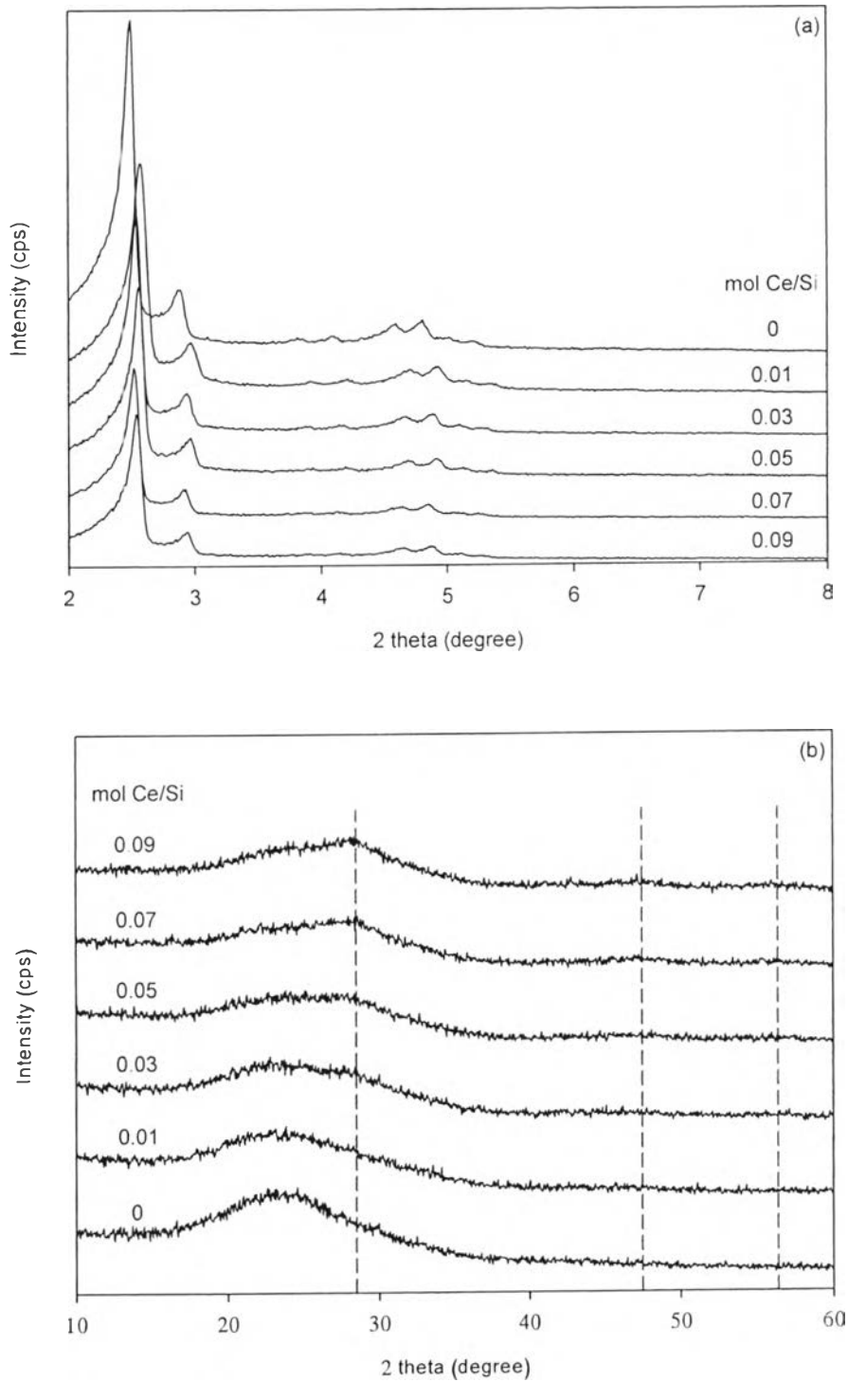

Figure 4.2 The XRD patterns of the calcined Ce-MCM-48 samples with different Ce contents over the range of (a) 2 theta = 2°–8° and (b) 2 theta = 10°–60°.

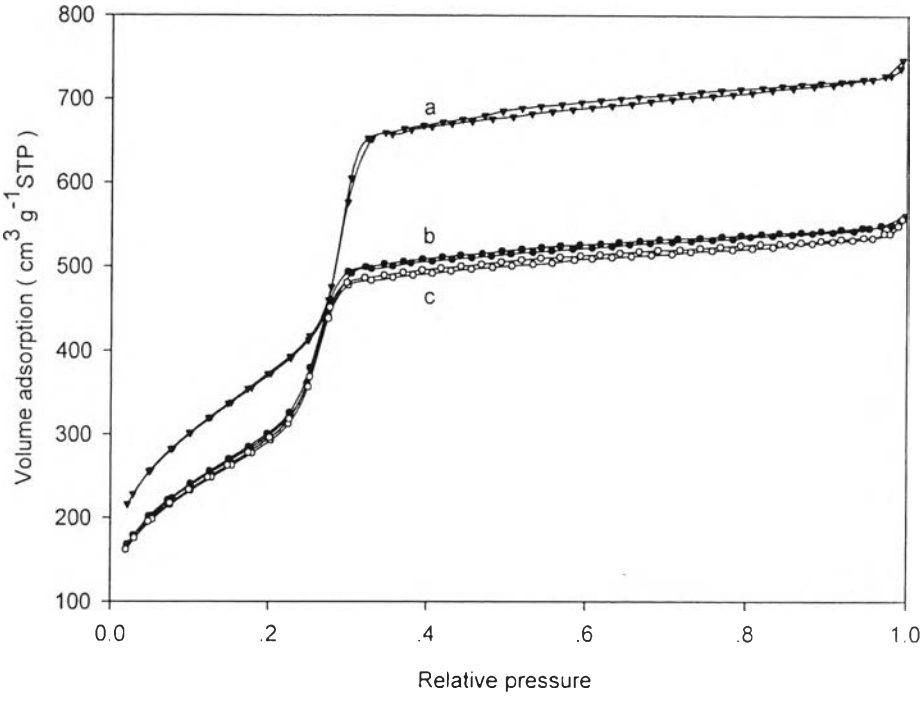

(a)

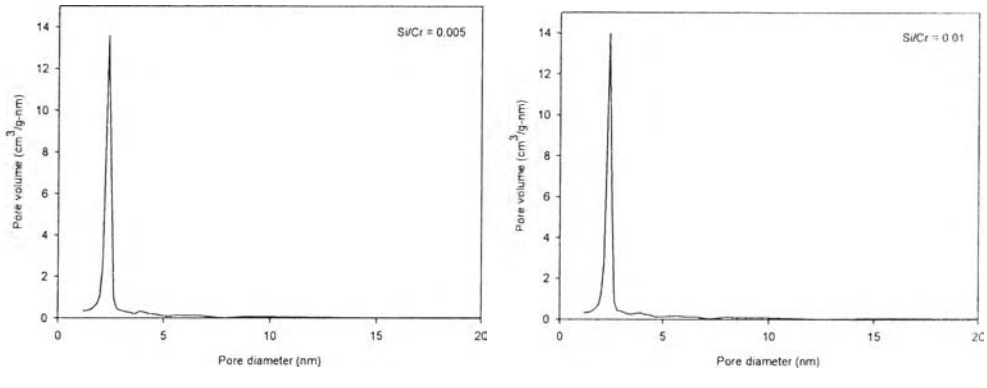

(b) (c)

Figure 4.3 The N_2 adsorption and desorption isotherms and the BJH pore-size distributions (calculated from desorption branch of isotherm) of calcined Cr-MCM-48 with different Cr/Si ratios of (a) 0, (b) 0.005 and (c) 0.01.

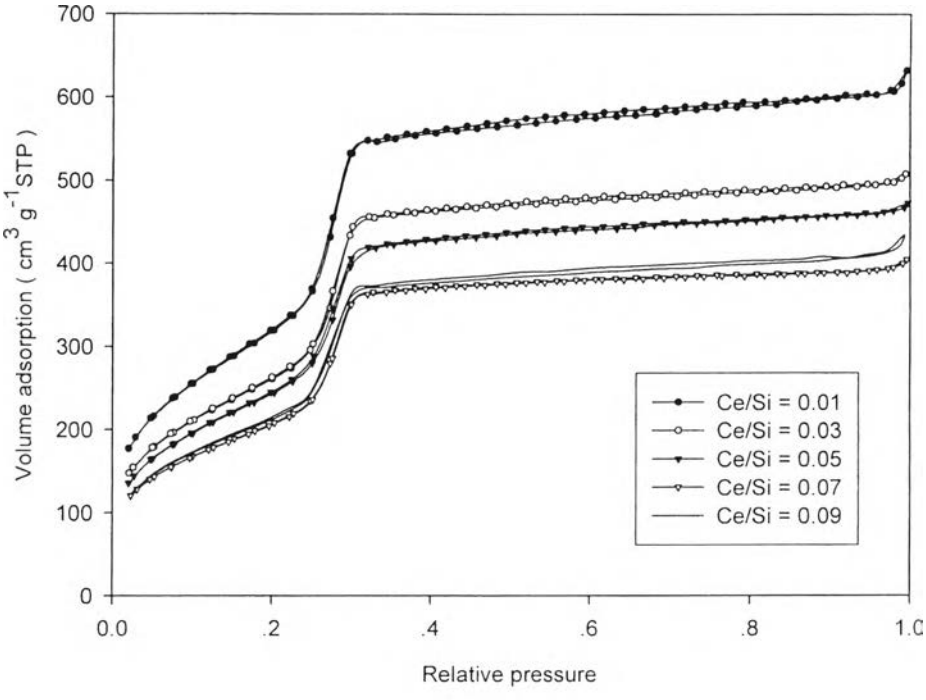

(a)

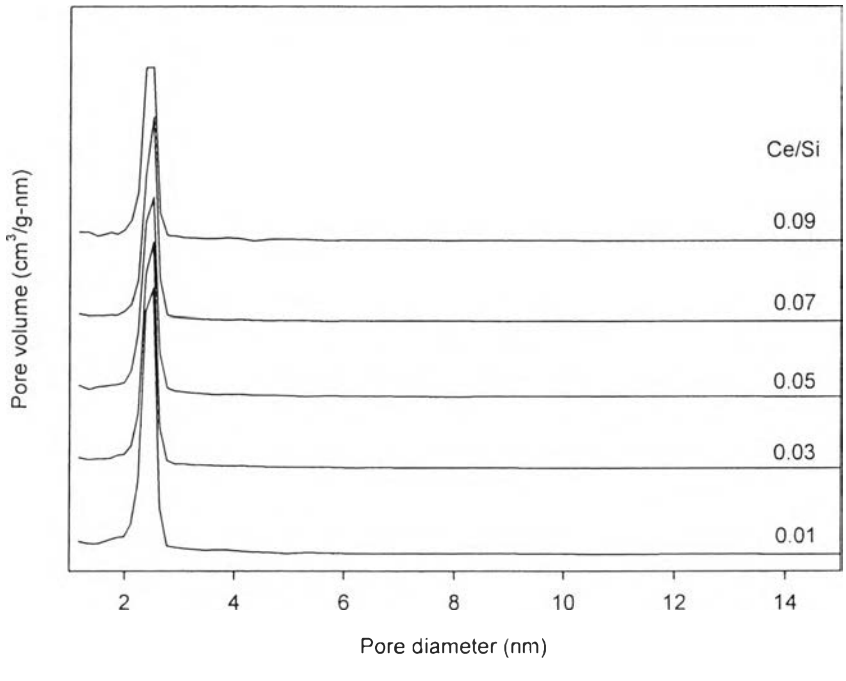

(b)

Figure 4.4 (a) The N_2 adsorption and desorption isotherms and (b) the BJH pore-size distributions (calculated from desorption branch of isotherm) of calcined Ce-MCM-48 with different Ce/Si ratios.

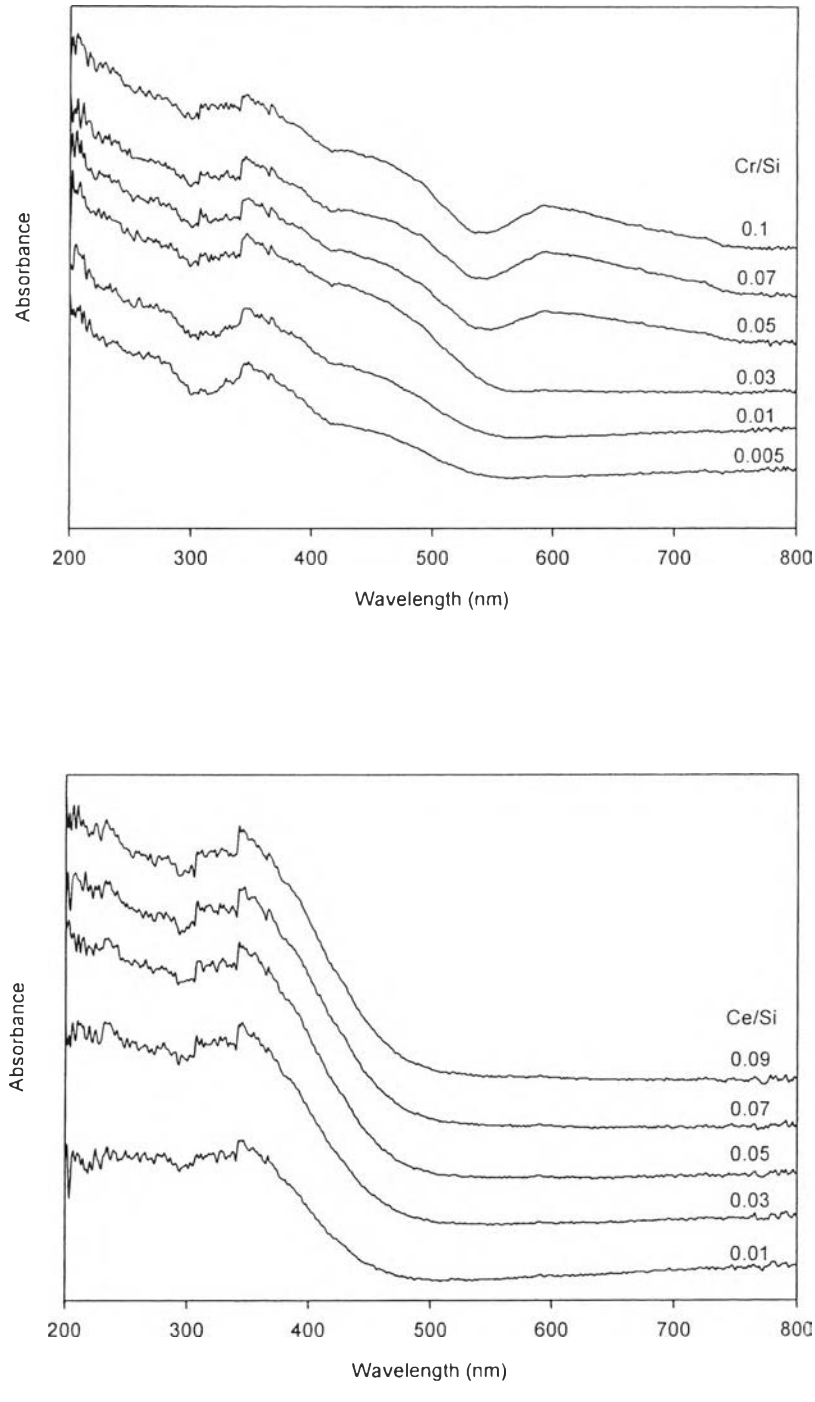

Figure 4.5 DR-UV-Vis spectra of calcined Cr-MCM-48 and Ce-MCM-48 with different Cr/Si and Ce/Si ratios.

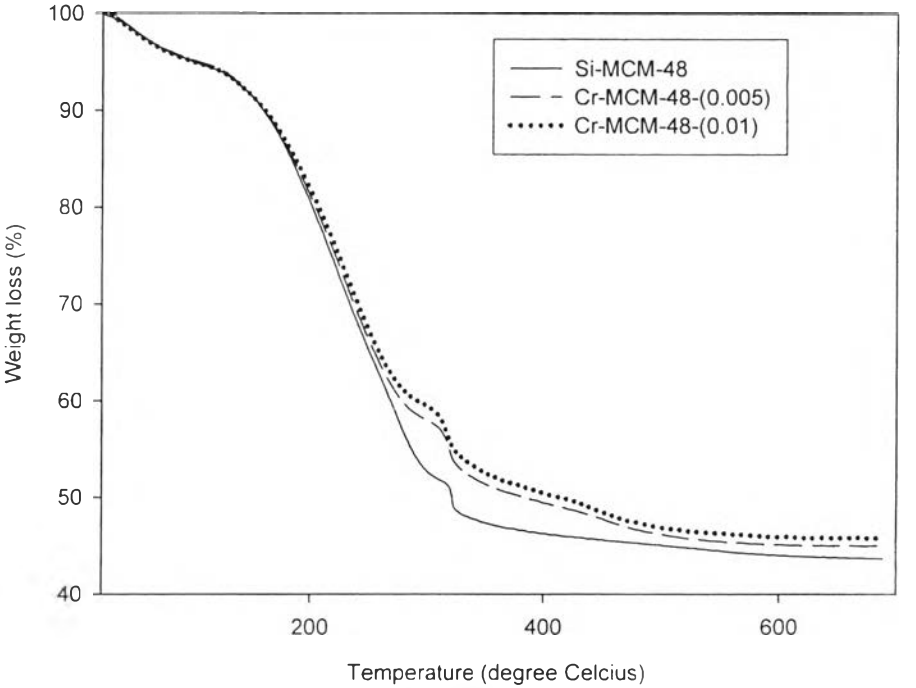
Si-MCM-48
Cr-MCM-48-(0.005)
Cr-MCM-48-(0.01)
Weight loss (%)
Temperature (degree Celcius)
100
90
80
70
60
50
40
200
400
600

(a)

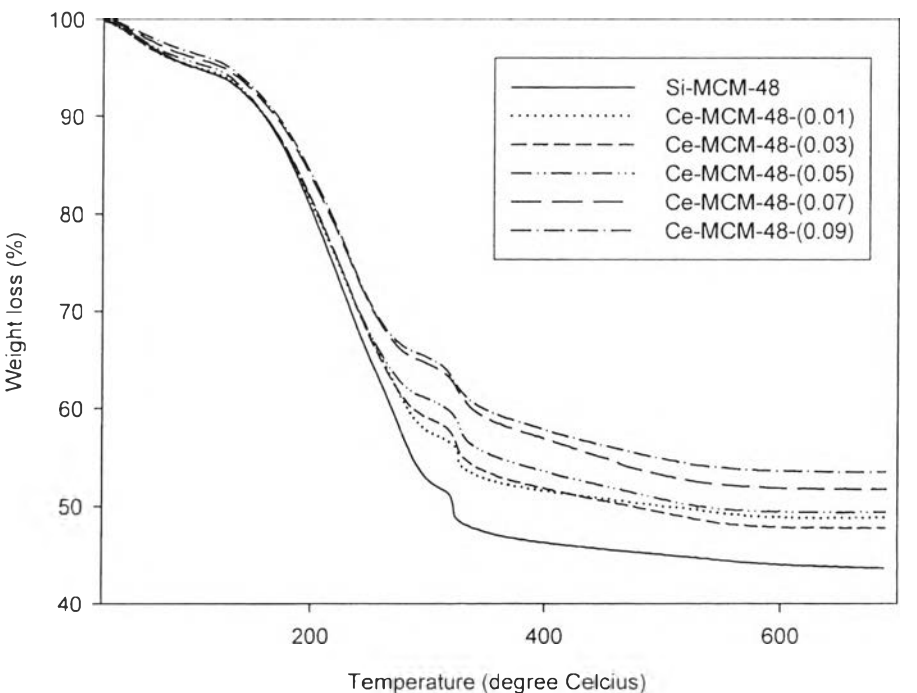
Si-MCM-48
Ce-MCM-48-(0.01)
Ce-MCM-48-(0.03)
Ce-MCM-48-(0.05)
Ce-MCM-48-(0.07)
Ce-MCM-48-(0.09)
Weight loss (%)
Temperature (degree Celcius)
100
90
80
70
60
50
40
200
400
600

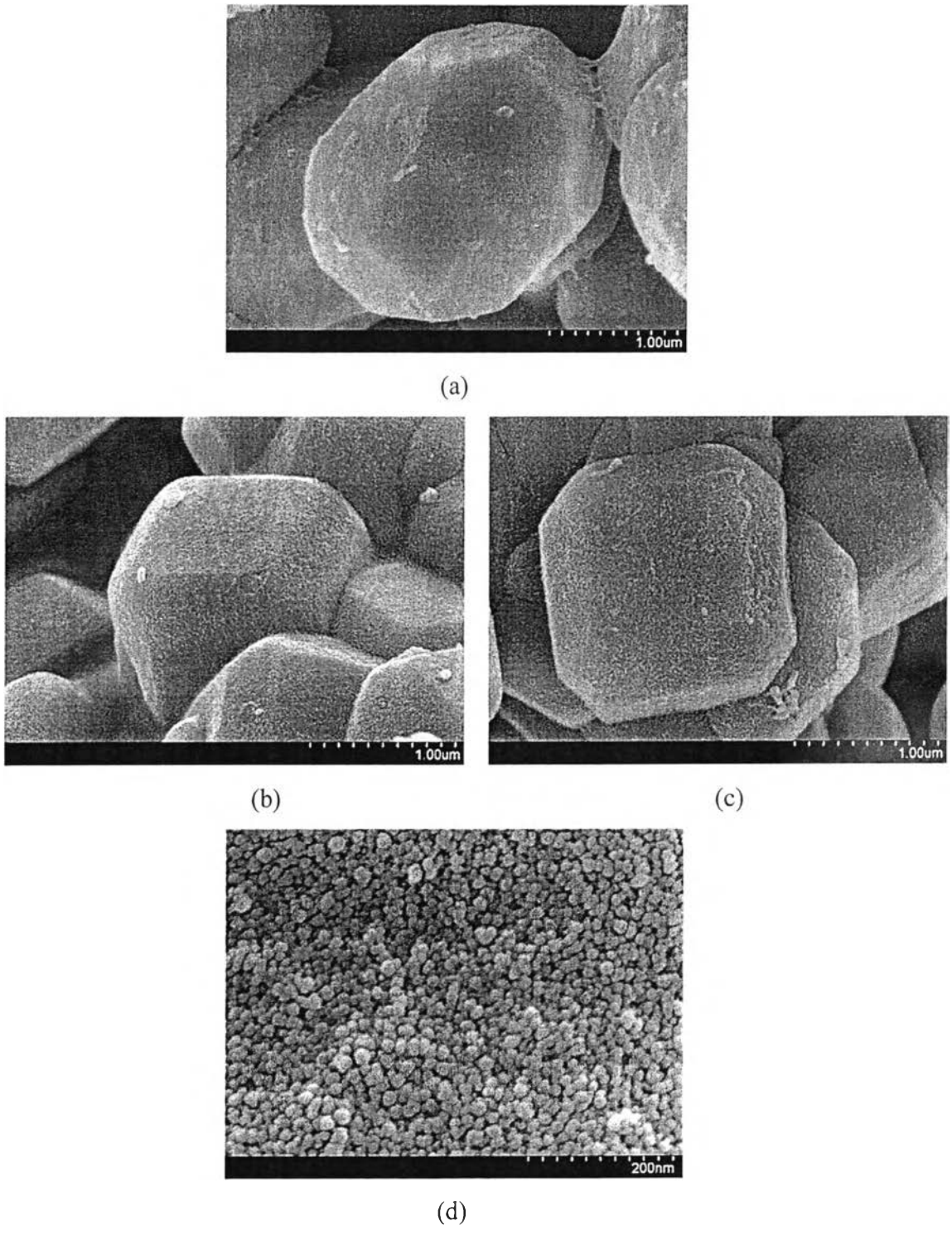

Figure 4.7 SEM images of (a) MCM-48 (x35000), (b) Cr-MCM-48 (0.005, x40000), (c) Cr-MCM-48 (0.01, x40000), and (d) Cr-MCM-48 (0.005, x200000).

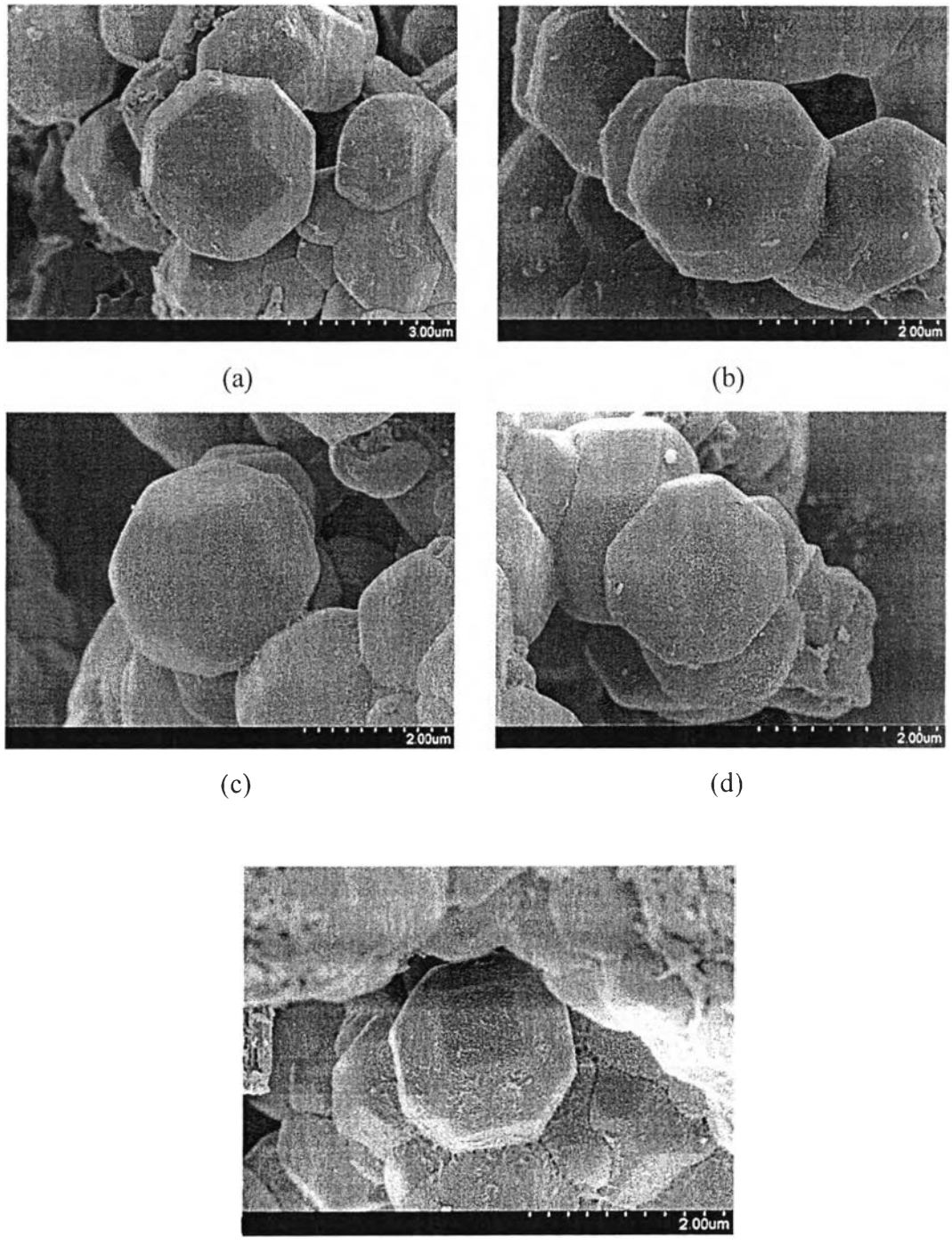

Figure 4.8 SEM images of Ce-MCM-48 with the Ce/Si ratio, y, of (a) 0.01, (b) 0.03, (c) 0.05, (d) 0.07, and (e) 0.09.

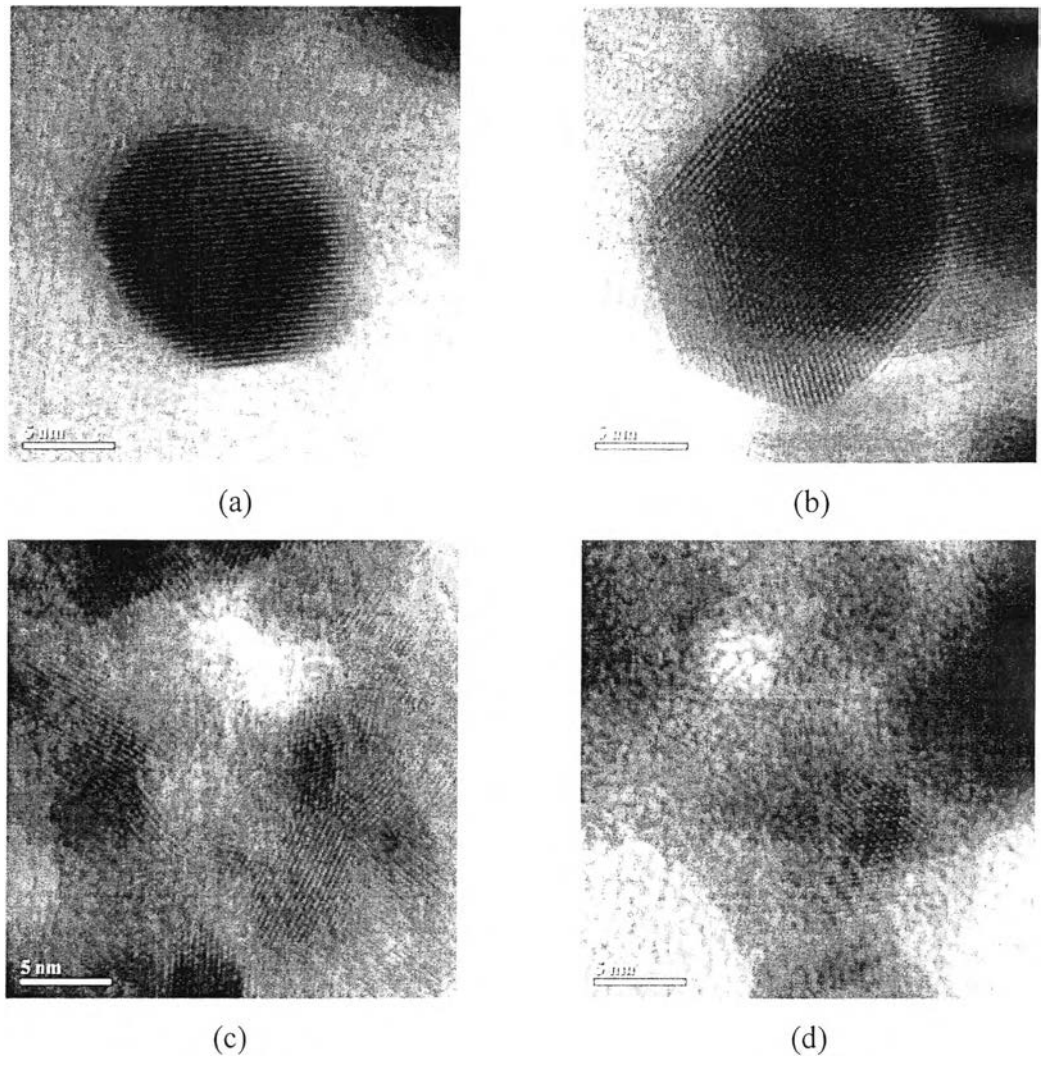

Figure 4.9 TEM images of Cr-MCM-48 (0.005) with incident direction along (a) [100] and (b) [432]; and Cr-MCM-48-(0.01) with incident direction along (c) [100] and (d) projection of [100].

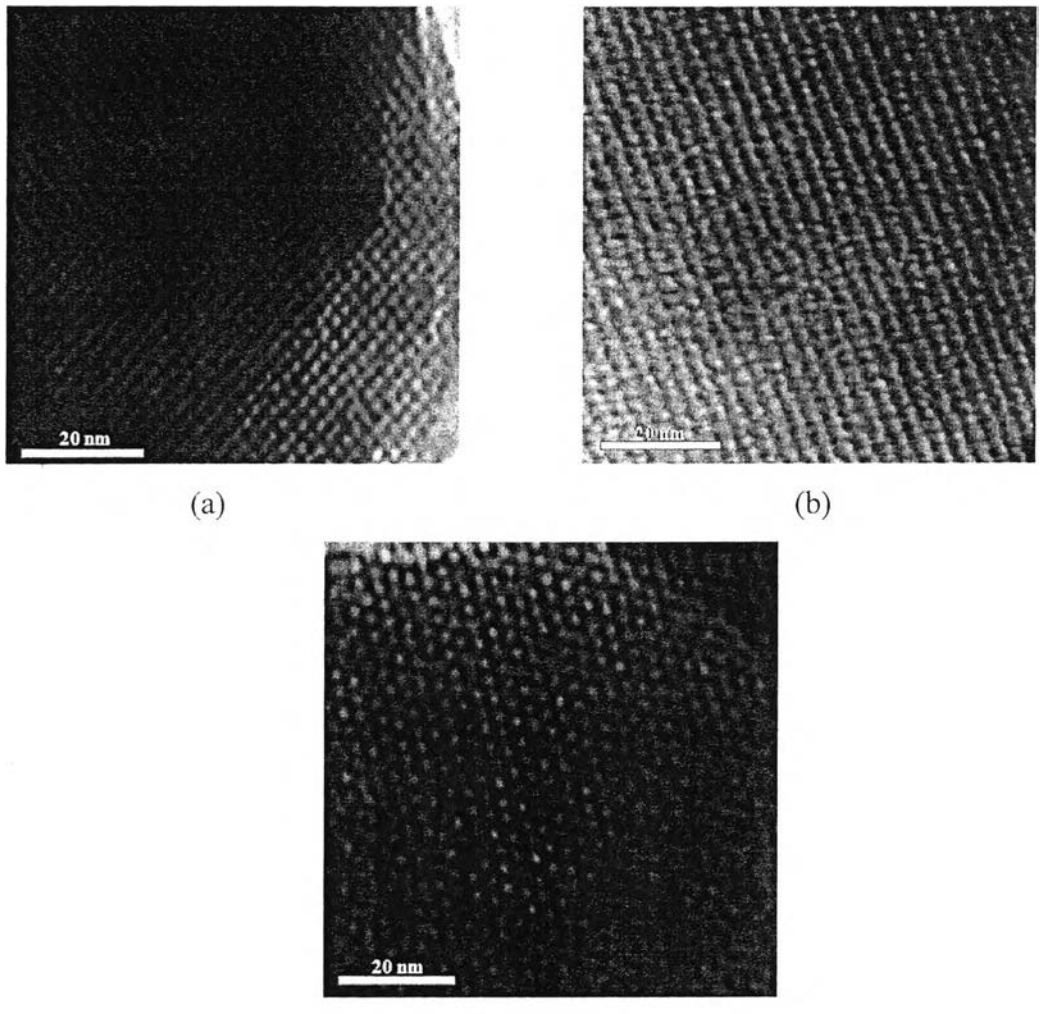

Figure 4.10 TEM images with incident direction along (a) [531], (b) [100] and (c) [111] of Ce-MCM-48-(0.01, 0.05 and 0.09), respectively.